Orientation Dependence in Molecular Dynamics Simulations of Shocked Single Crystals

Timothy C. Germann, Brad Lee Holian, and Peter S. Lomdahl
Theoretical Division, Los Alamos National Laboratory, Los Alamos, New Mexico 87545

Ramon Ravelo
Department of Physics, University of Texas, El Paso, Texas 79968-0515
(Received 1 February 1999)

We use multimillion-atom molecular dynamics simulations to study shock wave propagation in fcc crystals. As shown recently, shock waves along the ⟨100⟩ direction form intersecting stacking faults by slippage along {111} close-packed planes at sufficiently high shock strengths. We find even more interesting behavior of shocks propagating in other low-index directions: for the ⟨111⟩ case, an elastic precursor separates the shock front from the slipped (plastic) region. Shock waves along the ⟨110⟩ direction generate a leading solitary wave train, followed (at sufficiently high shock speeds) by an elastic precursor, and then a region of complex plastic deformation.

PACS numbers: 62.50.+p, 02.70.Ns, 62.20.Fe

The increasing capability for multimillion-atom molecular dynamics (MD) simulations, as well as experimental advances in resolving finer-scale features, permits the direct comparison of atomistic simulations with experiments. Recent large-scale simulations have given greater insight into the atomistic processes involved in crack propagation [1] and dislocation intersections [2]. Shock wave physics is becoming yet another fertile area for atomistic studies. Laser-driven shock waves through samples tens or hundreds of nanometers thick can be probed by spectroscopy [3] or interferometry [4] with picosecond time resolution, time and length scales well within the capabilities of modern MD simulations [5].

Previous studies of shock waves in 3D solids have primarily considered fcc Lennard-Jonesium with shocks traveling in the ⟨100⟩ direction [5–7]. An important first step to extending these simulations toward more realistic materials, which may include preexisting defects, dislocations, and grain boundaries, is the study of orientation-dependent effects on shock propagation in single crystals. In this Letter we report the first such systematic studies using molecular dynamics, including some surprising phenomena for ⟨111⟩ and ⟨110⟩ shocks which had not been seen in the ⟨100⟩ case, such as elastic precursors and complex modes of dislocation production. For comparison with earlier studies the results presented here are for the Lennard-Jones 6-12 spline pair potential described in Ref. [8]. However, we have also verified that the same generic behavior is found using a realistic embedded atom method (EAM) many-body potential for copper [9], though, of course, there are minor differences in details for pair vs many-body potentials, such as the equation of state and defect properties [5].

We use the SPaSM MD code [10], which enables routine simulations of 10^7 to 10^8 atoms on massively parallel machines, shared-memory multiprocessors, and even clusters of commodity personal computers. Shock waves are initiated by the same method which we have used elsewhere [5]: a perfect fcc crystal at some initial temperature T_0 travels at a uniform velocity $-u_p$ towards an infinitely massive stationary piston which specularly reflects any atoms reaching it. A shock wave then moves away from the piston at velocity $u_s - u_p$, where u_s is the planar shock velocity and u_p is the piston velocity. Periodic boundary conditions are applied in the lateral directions, with a free surface at the end of the sample farthest from the piston. System sizes of $50 \times 50 \times 200$ fcc unit cells (2×10^6 atoms) are typically used, although cross sections as large as 200×200 unit cells have been used with no observed change in behavior. A few simulations employed alternative methods for initiating shock waves, namely, shrinking periodic boundaries [11] or a momentum mirror composed of a few planes of cold, immobile atoms in the initial, uncompressed crystal structure.

Early ⟨100⟩ MD simulations with a few thousand atoms [6] as well as more recent simulations with up to 10×10^7 atoms [5] have exhibited shock-induced plasticity above a critical shock strength ($u_p \sim 0.2c_l$, where c_l is the longitudinal sound velocity, giving a strain ~13%), with slippage along {111} close-packed planes relaxing the shear stress. As anticipated by Smith [12] more than 40 years ago, pairs of Shockley partial dislocations are emitted from the shock front, leaving behind arrays of stacking faults on the four available {111} planes with nonzero resolved shear stress. Cross-sectional [100] planes exhibit irregular cross-hatch patterns, as shown in the top panel of Fig. 1. The mean spacing between stacking faults decreases with increasing u_p, providing a quantitative measure of shock-induced plasticity which is found to follow closely the total volumetric strain u_p/u_s across the shock front [5]. The intersecting stacking faults form locks which can remain stable (on the picosecond MD time scale), even if the shock wave is allowed to reflect off the free end as a rarefaction fan and return through the plastically deformed region.

Assuming a similar mechanism to be operating in the ⟨111⟩ and ⟨110⟩ cases, one would expect to see a pattern

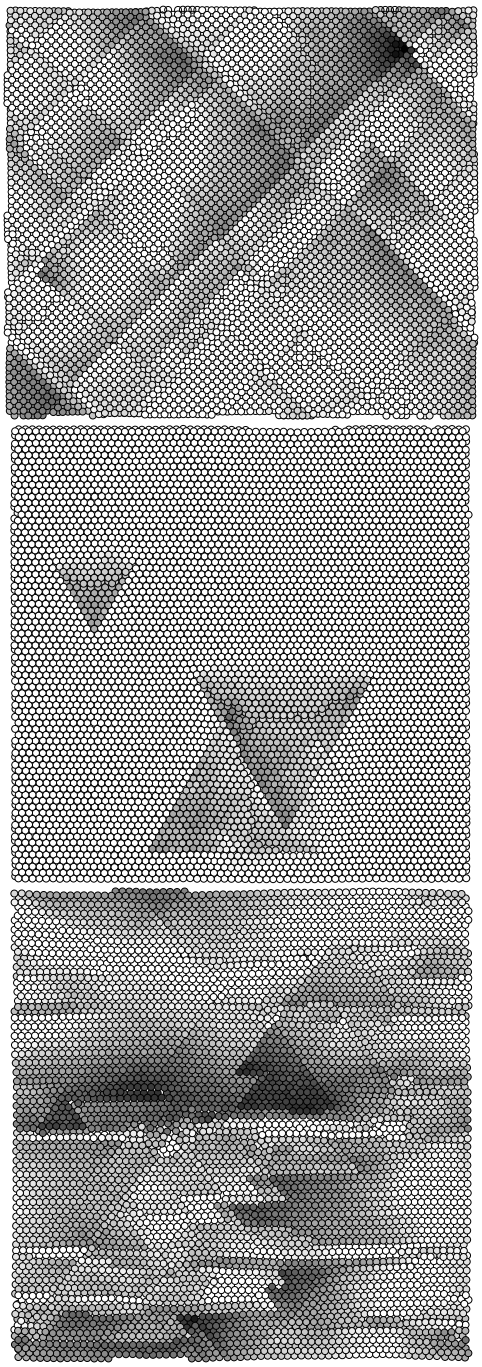

FIG. 1. From top to bottom, cross-sectional images near the rear end of the sample for ⟨100⟩, ⟨111⟩, and ⟨110⟩ shocks, respectively. Atoms are shaded in proportion to the transverse displacement from their initial lattice positions, up to one nearest-neighbor spacing r_0 ($1.5r_0$ for ⟨110⟩). Shrinking periodic boundary conditions were used, with a piston velocity $u_p = 0.2c_l$, where c_l is the longitudinal sound velocity for each direction: $\sqrt{72}$, $\sqrt{96}$, and $\sqrt{90}$, respectively.

of stacking faults on each {111} slip system with a nonzero resolved shear stress, for piston velocities above a certain threshold. In the ⟨111⟩ case three such planes are available, forming a triangular pattern on the [111] surface, while for ⟨110⟩ only two such planes are available, intersecting the [110] surface parallel to each other along the $\langle 1\bar{1}0\rangle$ axis. Indeed, in Fig. 1 we do find a triangular pattern of stacking faults in the ⟨111⟩ case, but the ⟨110⟩ case is quite different. Here instead of simple parallel stacking fault lines (which should be horizontal as shown here), we find a more complicated pattern of localized slippage along all four {111} planes, even for shock strengths barely above the threshold, as shown here (cf. Fig. 4). Since the two {111} planes inclined to the [110] surface can only relax the shear stress in the ⟨001⟩ direction, slippage must also occur along the two planes normal to the surface (at $\pm 30°$ from vertical in Fig. 1) to relax the shear stress in the $\langle 1\bar{1}0\rangle$ direction [13].

Shuffle-type martensitic transformations, which can relax the uniaxially compressed ⟨110⟩ orthorhombic structure to a (nearly) isostatically strained fcc crystal, have been proposed by Hirth *et al.* [14]. In our simulations, we see some evidence of this martensiticlike deformation when the piston is represented by a perfectly flat momentum mirror. At the confined surface of the sample near these "mirrors," lateral surface reconstruction is possible, which may indeed proceed in a manner similar to the proposed martensiticlike mechanism. However, the actual bulk mode of plastic deformation, beginning about ten lattice planes away from the mirror piston, is no less complicated but can be separated from the issue of surface reconstruction by using the method of shrinking periodic boundaries to generate the shock wave. In this case, only the bulk deformation mechanism is observed, which can be described as follows: Viewed down the ⟨001⟩ axis, which is transverse to the ⟨110⟩ shock propagation direction, the deformation is preceded by shear along lines of atoms in the $\langle 1\bar{1}0\rangle$ direction. Slippage then occurs along {111}-type slip planes, producing the beginnings of stacking faults. The instability to $\langle 1\bar{1}0\rangle$ shear is short ranged, and slippages on different {111} planes spread at nearly the speed of sound, competing with each other and resulting in a very complicated pattern of plastic deformation, with crystal orientation fundamentally unchanged from the original ⟨110⟩. The inherent anisotropy of the elastic properties and geometric complexity of slip systems in the ⟨110⟩ crystal result in a far more intricate pattern of slippage than for the relatively more straightforward ⟨100⟩ and ⟨111⟩ crystals, though the basic ingredients are similar.

These ⟨110⟩ results will be amplified in a forthcoming paper [15], where adiabatic compression simulations reveal the same kind of complex plastic deformation as seen in our shock wave computer experiments. Moreover, static ⟨110⟩ strain simulations show thermally activated deformation, which is identical in its generic structure. In the shock wave simulations, the profiles of the shear stress in both the ⟨111⟩ and ⟨110⟩ directions demonstrate this thermal activation, in that the shear stress relief initiates at the rearmost part of the shocked sample and propagates forward as a plastic wave. The activation or

induction time is responsible for the presence of an elastic precursor, wherein the uniaxial strain is compounded by small-amplitude transverse elastic distortions. We refer to them as "distortions" because of their reversible (elastic) nature, in contrast to essentially irreversible dislocation generation (plasticity). The elastic distortions in the precursor ultimately set the stage for the initiation of plastic flow. In contrast, the $\langle 100 \rangle$-direction plastic wave begins at the shock front after it has traveled 50–60 planes from the piston, whereupon it moves as partial dislocations both backwards to the piston and forward with the shock front in an overdriven, precursorless manner. The ease with which plastic flow is triggered roughly corresponds to the number of easily available $\{111\}$ slip systems: four for $\langle 100 \rangle$, three for $\langle 111 \rangle$, and two for $\langle 110 \rangle$.

Profiles of the shear and longitudinal pressure-volume tensor elements for the three shock directions are shown in Fig. 2. Each cross-sectional plane of the crystal contains $(7-20) \times 10^3$ atoms [$(6-12) \times 10^6$ atoms total], greatly reducing the noise seen in smaller simulations [6]. In all three cases the shock strength is above the threshold required to induce plasticity, allowing a comparison of the different ways in which the shear stress behind the shock front is relieved. For $\langle 100 \rangle$, the emission of partial dislocations at the shock front results in a drop in shear stress (though not completely to zero) immediately behind the front, as noted previously [5,6]. However, both the $\langle 111 \rangle$ and $\langle 110 \rangle$ cases exhibit an underdriven plastic wave which lags behind the elastic shock front, leaving an extended elastic precursor region in which the shear stress remains close to its maximum value. An atomic-level picture of this precursor is shown in Fig. 3. In the elastic precursor region, one particular set of $\{111\}$ planes exhibits a shear distortion, before finally nucleating dislocations at the plastic shock front, where irreversible slippage along all three available $\{111\}$ planes is observed.

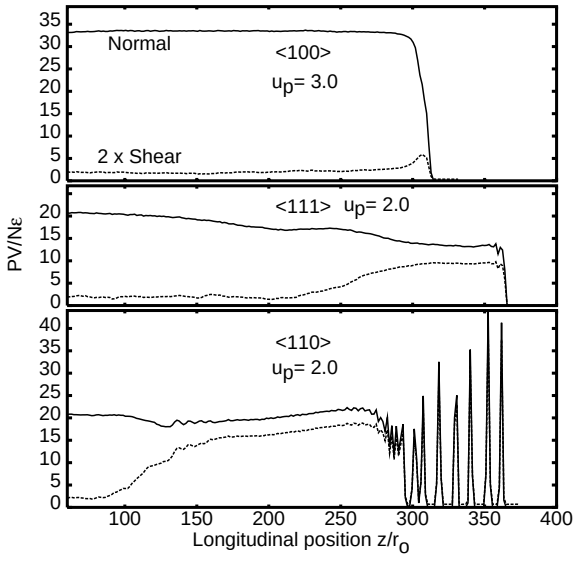

FIG. 2. Profiles of the longitudinal ($P_{zz}V$, solid line) and twice the shear ($[P_{zz} - (P_{xx} + P_{yy})/2]V$, dashed line) pressure-volume tensor components, in units of the bond energy ϵ. Shocks are propagating from left to right. Velocities are in reduced Lennard-Jones units, $\sqrt{\epsilon/m}$, where m is the atomic mass.

In addition, the $\langle 110 \rangle$ shocks exhibit a leading solitary wave train, spreading out as time progresses, which is not found in the other cases. Each "soliton" pulse is a compressive zone roughly three lattice planes wide, with atoms displaced primarily along the shock direction and very little, if at all, in the transverse directions. This effectively one-dimensional phenomenon has been observed in 1D shock simulations, for instance, in Toda lattices [16] and the even simpler case of a one-dimensional chain of hard rods [17]. Since this behavior results from the elastic bouncing of atomic planes off one another, only the repulsive potential wall is important, rather than the details of the attractive potential. Thus $\langle 110 \rangle$ solitary wave trains are seen for both Lennard-Jones and EAM potentials. What is somewhat surprising in the present case is that the solitary waves remain stable up to $T_0 \simeq T_{\mathrm{melt}}/10$, whereas such nonsteady wave trains are seen only along the $\langle 100 \rangle$ direction if the initial temperature is zero [18]. The $\langle 110 \rangle$ solitary waves could, however, be scattered by collisions with defects in real crystals, and their existence could be very sensitive to the crystal orientation relative to the shock propagation direction.

Shock velocities are measured by fitting longitudinal velocity profiles to a smoothed step (hyperbolic tangent) function at each front, tracking their positions until a steady wave velocity $u_s - u_p$ is reached. Elastic and plastic velocities u_s are shown as a function of piston velocity u_p in Fig. 4. Unlike the $\langle 100 \rangle$ case, where an overdriven plastic wave results in a linear relationship between the shock velocity u_s and piston velocity u_p over the entire range of u_p under consideration (nearly up to the point at which the sample melts), the underdriven plastic wave and elastic precursor for $\langle 111 \rangle$ and $\langle 110 \rangle$ lead to a more complex relationship between these two wave velocities and the piston velocity. Once the piston velocity is sufficiently high to trigger plastic deformation, the slope of the elastic wave speed decreases as energy goes into the thermally activated plastic deformation which is initiated near the rear

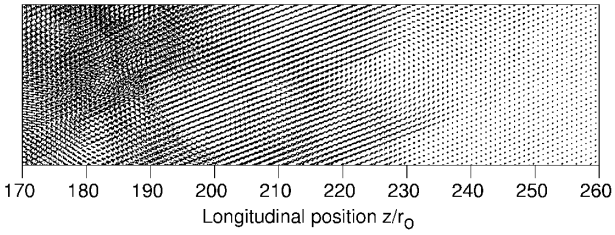

FIG. 3. Cross-sectional view of a $\langle 111 \rangle$ elastic precursor, showing both the elastic (near $z \simeq 230 r_0$) and plastic ($z \simeq 195 r_0$) shock fronts. Atoms are shown as dots, so that one can see through all 120 $[1\bar{1}0]$ planes of this simulation.

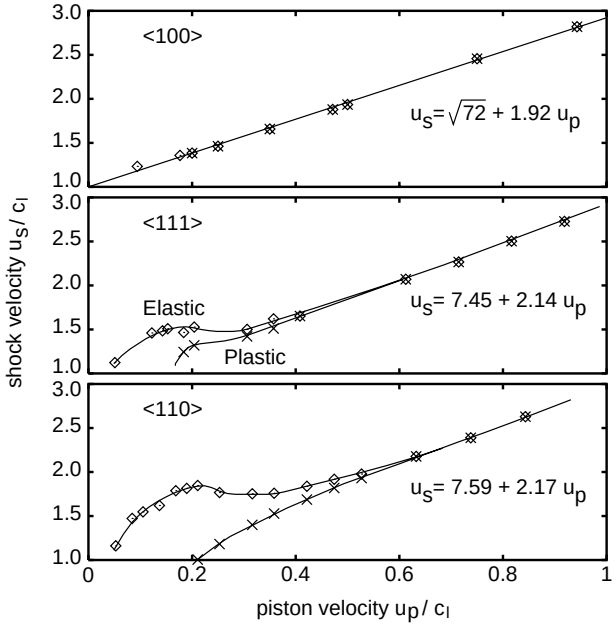

FIG. 4. Shock velocities as a function of piston velocity. Elastic wave velocities are denoted by diamonds and plastic ones by crosses, with both symbols being overlapped in the case of overdriven plastic waves. The approximate linear relationships in the strong-shock limit are given.

of the shocked sample. As the piston velocity is further increased, the width of the elastic precursor region steadily decreases as the plastic wave speed approaches the elastic speed, eventually resulting in an overdriven plastic wave for piston velocities greater than one-half the longitudinal sound velocity. Similar behavior, with either single or split shock waves depending on the piston velocity, has been noted in 2D simulations of a diatomic molecular solid which undergoes a phase transition to a close-packed solid at high pressures [19].

The critical shock strengths may be compared to those for smaller systems which are uniformly compressed along each of the three crystallographic orientations of interest [15]. The critical strain at which the system yields plastically (and the resolved shear stress [20] drops) is near 15% for the $\langle 100 \rangle$ and $\langle 111 \rangle$ directions, and 10% for the $\langle 110 \rangle$ direction, and the maximum resolved shear stresses are $3.5\epsilon/r_0^3$, $9.4\epsilon/r_0^3$, and $11.2\epsilon/r_0^3$, respectively. These static results agree reasonably well with the maximum shear stresses at the critical shock strength obtained from the present simulations, which are $4.2\epsilon/r_0^3$, $7.1\epsilon/r_0^3$, and $10.6\epsilon/r_0^3$, respectively. (For comparison, the tetragonal shear modulus is $(C_{11} - C_{12})/2 \simeq 20.8\epsilon/r_0^3$.)

In summary, we have carried out the first systematic MD study of shock waves in fcc single crystals in directions other than $\langle 100 \rangle$, finding surprising new phenomena which would not have been anticipated from earlier work [5–7], and showing that there is still much to learn about shocks in single crystals before we can expect to understand their behavior in imperfect or polycrystalline materials. This first appearance of elastic precursors, known to exist in real materials, is reassuring after their persistent absence in $\langle 100 \rangle$ simulations. On the other hand, both the stable solitary wave trains and the complexity of the deformation found for $\langle 110 \rangle$ shocks are quite unexpected, and it will be interesting to see whether future experiments on oriented single crystals and polycrystals will exhibit similar behavior.

This work was carried out under the auspices of the U.S. Department of Energy. Computations were performed using Cray/SGI Origin 2000s in the Advanced Computing Laboratory and Sun Enterprise 4000s in the Theoretical Division at Los Alamos. We thank J. P. Hirth, R. G. Hoagland, and S. V. Zybin for several useful discussions.

[1] S. J. Zhou *et al.*, Phys. Rev. Lett. **78**, 479 (1997); A. Omeltchenko *et al.*, Phys. Rev. Lett. **78**, 2148 (1997); D. Holland and M. Marder, Phys. Rev. Lett. **80**, 746 (1998); **81**, 4029(E) (1998).
[2] S. J. Zhou *et al.*, Science **279**, 1525 (1998).
[3] D. D. Dlott, S. Hambir, and J. Franken, J. Phys. Chem. B **102**, 2121 (1998).
[4] R. Evans *et al.*, Phys. Rev. Lett. **77**, 3359 (1996).
[5] B. L. Holian and P. S. Lomdahl, Science **280**, 2085 (1998).
[6] B. L. Holian, Phys. Rev. A **37**, 2562 (1988).
[7] V. V. Zhakhovskii *et al.*, Phys. Rev. Lett. **83**, 1175 (1999).
[8] B. L. Holian *et al.*, Phys. Rev. A **43**, 2655 (1991).
[9] A. F. Voter, Phys. Rev. B **57**, 13 985 (1998).
[10] P. S. Lomdahl *et al.*, in *Proceedings of Supercomputing 93* (IEEE Computer Society Press, Los Alamitos, CA, 1993), pp. 520–527; D. M. Beazley and P. S. Lomdahl, Parallel Comput. **20**, 173 (1994).
[11] B. L. Holian *et al.*, Phys. Rev. A **22**, 2798 (1980).
[12] C. S. Smith, Trans. Metall. Soc. AIME **212**, 574 (1958).
[13] J. D. Kiely and J. E. Houston, Phys. Rev. B **57**, 12 588 (1998).
[14] J. P. Hirth *et al.*, Acta Mater. **47**, 2409 (1999).
[15] R. Ravelo, B. L. Holian, and T. C. Germann (to be published).
[16] B. L. Holian, H. Flaschka, and D. W. McLaughlin, Phys. Rev. A **24**, 2595 (1981).
[17] B. L. Holian and G. K. Straub, Phys. Rev. B **18**, 1593 (1978).
[18] B. L. Holian and G. K. Straub, Phys. Rev. Lett. **43**, 1598 (1979).
[19] D. H. Robertson, D. W. Brenner, and C. T. White, Phys. Rev. Lett. **67**, 3132 (1991).
[20] The resolved shear stresses, in computational cell coordinates where z is the shock direction, are $\tau_{100} = [\sigma_{zz} - \frac{1}{2}(\sigma_{xx} + \sigma_{yy})]/\sqrt{6}$, $\tau_{111} = \sqrt{2/27}\,(\sigma_{zz} - \sigma_{yy})$, and $\tau_{110} = (\sigma_{zz} - \sigma_{xx})/\sqrt{6}$.